Oxidation during fuel-coolant interaction Advances and modeling

V. Loisel, J.-A. Zambaux, M. Hadj-Achour, S. Picchi, O. Coindreau, R. Meignen

Oxidation during Fuel-Coolant Interaction: advances and modeling

V. Loisel[+], J.-A. Zambaux*, M. Hadj-Achour*, S. Picchi*, O. Coindreau*, R. Meignen*[@]
[+] AREVA NP, 1, place de la Coupole - Jean-Millier - 92400 Courbevoie, France
*Institut de Radioprotection et de Sûreté Nucléaire (IRSN), Saint Paul Lez Durance, 13115, France
[@] corresponding author, renaud.meignen@irsn.fr

ABSTRACT

Following the OECD SERENA phase 2 program and EC SARNET-2 network conclusions, oxidation was identified as a major issue for a comprehensive modelling of Fuel Coolant Interaction (FCI). Indeed, the topic is very complex, involving hydrogen and void generation, strong heat release and change of material properties, in particular regarding solidification. Based on a literature review and recent experimental data, the mechanisms related to oxidation are revisited. Following this work, a kinetic model of oxidation is being built and applied to the thermohydraulic code MC3D, based on the competition between H_2/vapor inter-diffusion in the boundary layer and oxygen diffusion in the melt. Two drop configurations are considered here, in subcooled water and in superheated steam. Faced with the paucity of experimental data in terms of kinetics of reaction above the metal melting point, direct numerical simulations are performed in order to compare the reaction rates with those given by the macroscopic model and to provide a local scale observation of the boundary layer surrounding the drop during the process of oxidation.

KEYWORDS
FCI, Oxidation, Numerical Simulations

1. INTRODUCTION

During the progression of a severe accident with core melt in a nuclear reactor cooled with water, the relocation of the corium melt in the lower head may occur. The corium behavior in the lower head is currently the object of an R&D at the international level in the frame of the Ex-Vessel Retention (EVR) strategies, and in particular in the H2020 IVMR project (Fichot, et al., 2018). It is expected that the liquid corium in the lower head will stratified in two or three layers with one being essentially oxidic, and one or two being essentially metallic. A most probable scenario is that the upper layer is formed with light metals with a temporarily quite high superheat. This layer would easily attack the vessel and break it through, resulting in the flow in the reactor cavity of this superheated metallic melt. A second possibility is the failure of the vessel by the bottom layer composed with heavy superheated metals. If the vessel comes to fail, and if the pit is flooded with water (a condition for the EVR strategies), the melt is then expected to flow out of the vessel with a metallic composition at first, inducing oxidation. Ex-vessel FCI is also an issue for the cases of BWR's with large (flooded) pit. Apart from a massive hydrogen release, there are three effects of oxidation on FCI. On the one hand, experimental evidences (Cho, Armstrong & Gunther, 1998) have shown that the potentially high amount of released chemical energy can contribute to increase the magnitude as well as the duration of the steam explosion. On the other hand, the hydrogen generation can substantially increase the void fraction during the premixing, which could limit to possibility to trigger a steam explosion. On a side note, the oxidation process is also responsible for the change in the material properties that can affect its coolability and solidification. Indeed, the strong explosions reported by Cho, Armstrong & Gunther could be obtained only with a fast triggering, before

the melt jet solidifies. This behavior is interpreted as being essentially due to an increase of the solidification temperature bounds (solidus and liquidus) during the oxidation process.

Oxidation is also an issue regarding oxidic U-Zr-O melts. The U-Zr-O system is currently the field of efforts to clarify its behavior at high temperatures. Indeed, UO_2/ZrO_2 melts, as classically used for "prototypical" corium may slightly over-oxidize (Mastromarino et al., 2017). This behavior could be noticed in the FARO experiments using UO_2/ZrO_2 melts and for which a production of hydrogen could be measured (Magallon, Huhtiniemi & Hohmann, 1999). For this system, the question of hydrogen production and energy release is not so important, but the change of composition affects the solidification properties and hence, should be taken into account in the models and calculations.

In the framework of nuclear safety, oxidation of metals in water and steam has been studied extensively for decades, resulting in an exhaustive database of reaction rates for metals at relatively low temperatures (*i.e.* at solid state). On the other hand, much less is known concerning temperatures above the melting point. First experimental works dealing with the hazards potentially induced by melt oxidation during the course of a Fuel-Coolant Interaction (FCI) date back to the 1950s and have evaluated the possibility of an explosive event under these conditions. In order to provide basic data, Bostrom (1954), Lemmon Jr. et al.(1957) and Baker Jr & Just (1962) conducted experiments dedicated to the evaluation of oxidation rates of zirconium (or zircaloy) in both steam and water. Based on the results obtained, most of the theoretical models subsequently developed assumed that the kinetic of oxidation is governed either by vapor diffusion in the boundary layer, if the material remains fully melted, or by oxygen diffusion if the fuel is solid at the interface (Corradini, Mitchell & Evans, 1983) (Young, Berman & Pong, 1988) (Lee, Park & Chung, 1997). More recently, two sets of experiments were conducted by Cho, Armstrong & Gunther, (1988) with melts containing zirconium with steel or with zirconia at various ratios. As already explained, explosions took place in the triggered experiments only, otherwise rapid quenching and solidification was observed. The strengths of the explosions were directly linked to the amount of zirconium, which could be nearly totally oxidized during the explosions.

Interaction of aluminum with water has also been the subject of several works, in general motivated by the fact that aluminum is used in the core of various research and military nuclear reactors but also by the numerous accidents occurring in metal cast industries. The observations (e.g. (Nelson, 1995) for a synthesis) of strong and fast explosions accompanied by strong and fast oxidation triggered a number of theories and papers. In particular, Epstein and co-workers attempted to explain the fact that surface oxidation could not produce a stable barrier to further oxidation at temperatures nearly down to the melting point. However, these works focused mostly on the explosion whereas only few data are available for non-explosive drops, to support the development oxidation kinetic models.

Corradini et al. (1983) developed a model included in the TEXAS code to evaluate the kinetics of oxidation for three different configurations: coarse mixing, steam explosion and stratified melt quenching, without considering the impact of solidification. Later on, this model has been reworked by Young, Berman, & Pong (1988) to correct mistakes, which caused a diminution of the calculated reaction rates. However, the corrected version gives much larger amounts of hydrogen than that of the experimental results, and the model no longer describes a significant difference between the different configurations. To overcome this issue, the mechanistic model of Lee, Park, & Chung (1997) accounts for the formation of an oxide coating. Although this improvement permitted a much better agreement with the experimental data the situation appears quite confusing on both understanding and modeling aspects. Indeed, the impact of the modeling depends primarily on the simulation of the FCI itself (drop size and local flow configuration), on which some confidence has been recognized only recently (Meignen et al, 2014).

This present work aims at readdressing this question with the help of recent analyses and experiments, and proposing a new model of oxidation specifically designed for dealing with the various stages of FCI

with the thermal-hydraulic code MC3D (Meignen et al., 2014) (Meignen, Raverdy, Picchi & Lamome, 2014). The verification of the model was confronted to the lack of precise experimental data for the oxidation phenomena itself in FCI conditions. To overcome this difficulty, a work of fine numerical simulations at the drop scale (quasi DNS) has also been engaged. The paper discusses the advances of the work, still limited regarding the necessary verification work against explosion experimental data.

2. PHYSICAL AND MATHEMATICAL MODELLING

2.1. Phenomenology

2.1.1. Fuel-Coolant Interaction

The contact between the melt and the water heralds the beginning of the fuel-coolant interaction. A recent status of FCI understanding and modeling capabilities is given by Meignen et al. (2014). It is recognized that, in most cases, the mixing phase starts with the melt fragmentation into coarse drops of millimetric sizes. This fragmentation is accompanied by vaporization, the intensity of which is mostly directed by the characteristic size of the fragmented melt. Also, oxidation would most likely occur for the fragmented or highly deformed parts of the melt. It is worth noting that the immediate neighborhood of the jet is mostly gaseous due to the significant amount of heat released during the quench. This is not necessarily the case in experiments but the recent simulations performed in the frame of the OECD SERENA-2 program (Meignen et al., 2014) indicates that, at reactor scale, i.e. for large jets (say larger than 10 cm), a large vapor film embeds the melt jet and a large fraction of the melt drops. The resulting molten drops are therefore created and remains for a substantial time in a vapor-rich environment before being convected into the water. Consequently, two configurations must be considered to track the time evolution of the melt oxidation all along the entire process (Fig. 1): when a drop is within an infinite medium of steam, and the film boiling configuration. It is nevertheless quite likely that, during premixing, the configuration of drop in gas is the most important regarding the effectiveness of oxidation. Indeed, the CCM experiments (Spencer, Wang, Blomquist, McUmber & Schneider, 1994), using a mixture of UO_2/ZrO_2 and stainless steel, indicated a much more effective oxidation in cases with saturated water, i.e. probably large void in mixture, than cases in subcooled water.

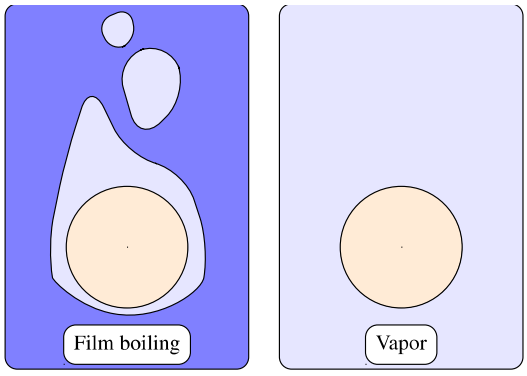

Fig. 1: Drop configuration studied in order to model oxidation

In contrast, during a steam explosion event, the flow configuration changes drastically. A large part of the void collapses due to the pressurization. Although at large scale (i.e. reactor application) the void around the jet cannot completely collapse, it is likely that the configuration of drop in liquid is the most important to take into account.

2.1.2. Oxidation process

The consensus adopted in the literature describes the process of oxidation according to three steps, each one having its own characteristic time. (1) The first of them consists to supply the reactive surface with steam. This can only be done if the vapor diffuses through the hydrogen that is being generated at the surface. (2) The next step is the atomic dissociation of the water molecules, which releases both hydrogen atoms and energy. (3) The final stage of the oxidation process describes on one side the absorption and diffusion of the oxygen atoms inside the material's body, and on the other side the recombination of the hydrogen atoms to form H_2.

It is well accepted that the second step is very fast is not a limiting process. It is also well accepted that H_2O/H_2 diffusion in gaseous boundary layers around the melt is a limiting process that must, in general, be accounted for. A first key issue is then to check at the third step to verify the ability of oxygen to be effectively rapidly diffused inside the melt. Other way, an oxidized layer may rapidly form and block the process. In such case, the oxide layer has very different physical and thermodynamical properties. In particular, it should induce in most cases the solidification of this layer. The solidification itself should in turn impose a faster decrease of the temperature in this layer, and so a slower oxidation rate.

During the premixing stage of the interaction, the typical length scale (R) of the fragmented melt is about 1 millimeter, and the typical time scale (τ) is about 1 s. The experiments involving oxidation for U-Zr-O melts (Magallon, Huhtiniemi, & Hohmann, 1999), (Tyrpekl, et al., 2015), U-Zr-SS-O melts (Spencer, Wang, Blomquist, McUmber, & Schneider, 1994), or Zr-SS-O melts (Cho, Armstrong, & Gunther, 1998) indicated that, during the premixing, the reaction was not necessarily completed but had at least a level of some % (up to about 30 % in saturated water). Thus, during this stage, a minimum diffusion coefficient (R^2/τ) of oxygen inside the melt of 10^{-7} to 10^{-6} m²/s may be required for partial or total oxidation. During the explosion, the typical length scale (R) of the fragmented melt during the premixing is less than 50 µm, and the typical time scale (τ) is about 1 ms. This implies that the minimum diffusion coefficient of oxygen in the melt for a complete oxidation may have to be as high as 10^{-6} m²/s.

At the moment, we will restrict our attention to Zr-O and U-Zr-O systems, despite the fact that, for ex-vessel reactor applications, the case of metal mixtures U-Fe-Zr should be more appropriate.

Regarding U-Zr-O melts, the detailed analysis of (Tyrpekl, et al., 2015) of some KROTOS tests, some with explosion, some without, Fig. 2, indicated a final over-stoichiometry ($(U\text{-}Zr)O_{2+y}$) rather homogenous, with y in between 0.11 and 0.17. This is consistent with recent thermodynamical studies of this system reported in (Mastromarino, et al., 2017) indicating that the solidus and liquidus temperatures of initially stoichiometric U-Zr-O particles are notably reduced when the melt exposed in oxidizing environment, with a final over-stoichiometry of about 0.1.

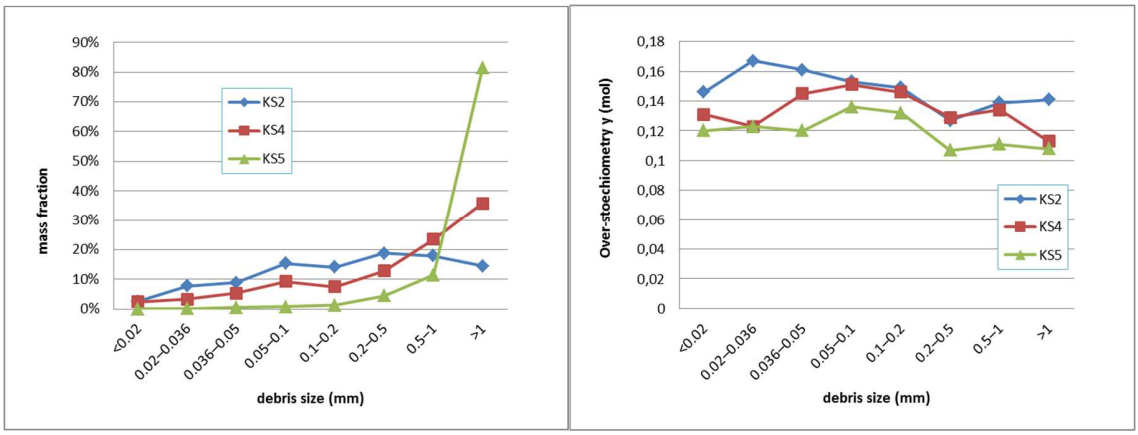

Fig. 2: Mass fraction for each size interval and corresponding mean over-stoichiometry in 3 KROTOS tests, from (Tyrpekl, et al., 2015)

The characteristic necessary diffusion coefficients discussed above are quite higher than those usually reported in the literature. The diffusion of oxygen in $UO_{2\pm x}$ was analyzed in detail by Breitung (1978) (see also (Berthinier, Rado, Chatillon & Hodaj, 2013)). For the considered temperatures (2500 – 3000 K), he could propose a chemical-diffusion coefficient (not to be confused with self-diffusion) of the order of 10^{-7} m²/s (self-diffusion coefficient of the order of 10^{-9} m²/s). Recently, applying the molecular dynamics theory, Yakub, Ronchi, & Staicu (2007) found similar values for the oxygen self-diffusion in UO_2 in liquid state.

Concerning the case of ZrO_{2-x}, the situation seems a bit confusing since there are several available data for self-diffusion with rather large differences, depending of the diffusion mode. Yakub et al. also analyzed the case of liquid ZrO_{2-x} and propose a law for self-diffusion. Our evaluation of the chemical diffusion, using Yakub's law and the NUCLEA database (e.g. (Barrachin, Chevalier, Cheynet & Fischer, 2008)) yields, for the case x=0.1 (i.e. $ZrO_{1.9}$) corresponding to the test KROTOS KS-5, also a value of the order of 10^{-7} m²/s.

Despite the abundant literature on Zr and zircaloy oxidation, experimental data relevant to oxygen diffusion in very high temperatures Zr could not be found. Extrapolations of diffusion data in zirconia in the range 1000-1500 K leads to chemical diffusion coefficients between 10^{-8} m²/s and 10^{-7} m²/s in the melting temperature range. Recently, the Molecular Dynamics method could be employed by (Mendelev & Bokstein, 2010) to produce a law for self-diffusion at high temperature, but still in solid phase, yielding similar values for the chemical diffusion.

Thus, for pure Zr, but also for $(U\text{-}Zr)O_{2\pm x}$ melts, although the values given above are compatible with a fast oxidation, an additional mechanism may be necessary to achieve oxidation as observed in the experiments. For zirconium, the strong release of energy might rapidly increase the temperature and thus increase the diffusion. However, an efficient mechanism in the liquid state is the movement of the fluid itself. The circulation alone in a spherical drop of fixed shape is not very efficient, although it may already multiply the diffusion by a factor 2 to 3. Much more effective are the oscillatory effects and local small scale turbulence. Several theories have been developed but require detailed knowledge of the local flow (see e.g. (Turney & Banerjee, 2013)). Of course, such detailed knowledge of the flow is out of reach in the current available FCI models, thus at present, the choice is to introduce a law of the form:

$$D = F(T).D_0(T)$$

where F is a numerical function of temperature tending to 1 when the melt is supposed to be solid, and $D_0(T)$ is the chemical diffusion coefficient (in the absence of fluid movement), obtained through thermodynamics analyses for the considered material.

At that point, it is important to discuss here another issue for FCI which is the solidification process. Some FCI models make the hypothesis that the solidification occurs mainly as crust growth at the surface of melt globules and MC3D also provides such model (Uršič, Leskovar, & Meignen, 2015) as an option. However, the mixing processes at liquid state previously discussed, due to surface stretching and local oscillations/turbulence, should also impact similarly the temperature diffusion. This is equivalent to multiply the conduction coefficient by one or two orders of magnitude so that, even oxides may behave as very conductive materials.

Oxidation and solidification are then strongly linked and a simplified modeling with homogenous oxidation grade and temperature inside the melt seems sufficiently accurate at first order.

2.2 Model of H_2 generation

2.2.1 General modeling

We will now focus our attention on the modeling of oxidation and hydrogen generation with the hypothesis that, at least in the liquid state, the main limitation process is the diffusion in the gas mixture surrounding the melt globule, either in gaseous environment, either in film boiling conditions.

Let's consider the oxidation of *x* moles of a melted metal drop Me by *y* moles of steam leading to the creation of hydrogen and the production (or consumption) of heat:

$$x \cdot \mathrm{Me} + y \cdot \mathrm{H_2O} \rightarrow \mathrm{Me}_x\mathrm{O}_y + y \cdot \mathrm{H_2}. \tag{1}$$

In agreement with the assumption stating that the oxidation kinetic is constrained by the vapor-H_2 inter-diffusion characteristic time, the hydrogen quantity produced, providing the vapor arriving at the interface has been consumed by the reaction, can be written in terms of a Fick's law:

$$\frac{\mathrm{d}\bar{m}_{\mathrm{H_2}}}{\mathrm{d}t} = D_{H_2/H_2O} \cdot M_{\mathrm{H_2}} \cdot \frac{\mathrm{d}c_{\mathrm{H_2}}}{\mathrm{d}r}, \tag{2}$$

where $\bar{m}_{\mathrm{H_2}}$ stands for the generated mass of hydrogen per unit of area (kg·m^{-2}) and $M_{\mathrm{H_2}}$ is the hydrogen molar mass (*i.e.* 2×10^{-3} kg·mol^{-1}). The vapor-H_2 inter-diffusion coefficient D (m^2·s^{-1}) has been experimentally determined by Furman (1959) as a function of the mixture temperature and pressure (expressed in atm):

$$D_{H_2/H_2O} = 6.52 \times 10^{-9} \cdot \frac{T_{\mathrm{m}}^{1.68}}{p_{\mathrm{atm}}} \tag{3}$$

The last term of (2) describes the gradient of hydrogen concentration ($c_{\mathrm{H_2}}$ in mol·m^{-3}) across the boundary layer surrounding the drop. Typical FCI conditions often involve a large temperature difference between the drops and the ambient fluid so that strong variations of the physical properties are expected across the boundary layer. Such conditions make the analytical determination of the temperature profile quite complex even if the weak mixture Prandtl number (Pr < 0.7) suggests that the velocity profile has a weak influence on that of the temperature. For that reason, this gradient of hydrogen concentration is

approximated by the differential of hydrogen concentration expressed across the boundary layer whose expression depends on the drop configuration, such as:

$$\frac{\mathrm{d}c_{\mathrm{H_2}}}{\mathrm{d}r} \approx \begin{cases} \dfrac{\Delta c_{\mathrm{H_2}}}{L_{\mathrm{c}}/_{\mathrm{Sh}}} & \text{(vapor)}, \quad (4a) \\ \dfrac{\Delta c_{\mathrm{H_2}}}{\delta} & \text{(film boiling)}. \quad (4b) \end{cases}$$

The approximation in eq. 4a uses a diffusional length L_c/Sh that involves a Sherwood number to characterize the mass transfer around the drop. Traditionally, L_c is the diameter of the sphere or the cylinder. As to the film boiling case (eq. 4b), $\Delta c_{\mathrm{H_2}}$ is determined over the distance defined between the drop surface and the liquid-gas interface, *i.e*. the gas-vapor film thickness δ. However, the film thickness n is not constant around the drop and no analytical expression has been proposed up to now in such conditions. Epstein and Hauser (1980) developed a way to evaluate this film thickness along with the heat transfers in the frame of a sphere or cylinder at high temperature submitted to a subcooled forced flow, the effects of oxidation not being accounted for. Epstein et al. (1984) later studied the implications of the hydrogen on the heat exchanges when generated in the surrounding film. Unfortunately, no explicit expression of the film thickness could be formally deduced. Therefore, the value of δ given by the Epstein-Hauser model will be used in a first place.
It may be noticed that these formulations do not account, once more, the effect of local oscillations and stretching of the surface. However, this may be achieved by the choice of adequate Sherwood numbers (or film equivalent thickness). The data are scarce and thus, at the moment, the modeling is based on the hypothesis of rigid drops.

The differential of hydrogen concentration mentioned above must be written accordingly to the drop configuration. At the gas-drop interface, we already have postulated that the incident steam is totally consumed by the reaction and then replaced by the hydrogen produced. Hence, the hydrogen partial pressure is equal to the total pressure p, and we have at the drop surface ($r = 0$):

$$c_{\mathrm{H_2}}\big|_{r=0} = \frac{p}{R \cdot T_{\mathrm{s}}}, \quad (5)$$

T_s being the surface temperature of the molten drop. At the other end of the thermal layer ($r = \delta_T$), the hydrogen concentration resulting to its diffusion away from the drop is:

$$c_{\mathrm{H_2}}\big|_{r=\delta_{\mathrm{T}}} = \frac{p_{\mathrm{H_2}}}{R \cdot T_{\infty}}. \quad (6)$$

This expression can only be valid for the vapor configuration. In the liquid configuration, the concentration of hydrogen is related to the conditions at the interface. These ones are not so clear. It is expected that an important production of vapor occurs at the interface, so one should be quite close to the saturation regarding total pressure. With such hypothesis, the hydrogen partial pressure can be neglected at the interface. However, this hypothesis needs further investigations.

2.2.2 Proposed formulations

Taking into account what has been previously stated, the formulation of the hydrogen production kinetic for a drop of diameter d subjected to a gaseous environment, can be written as follows:

$$\frac{\mathrm{d}\bar{m}_{\mathrm{H_2}}^{\mathrm{VAP}}}{\mathrm{d}t} = D \cdot M_{\mathrm{H_2}} \cdot \frac{\mathrm{Sh_{vap}}}{d} \cdot \left(\frac{p}{R \cdot T_{\mathrm{s}}} - \frac{p_{\mathrm{H_2}}}{R \cdot T_{\infty}}\right) \tag{7}$$

The Sherwood number used in this model is usually derived from common empirical heat transfer correlations such as that of (Ranz & Marschall, 1952)by considering the analogy between conduction-convection heat transfers and mass diffusion around a given geometry:

$$\mathrm{Nu_{RM}} = 2 + 0.6 \cdot \mathrm{Re}^{1/2} \cdot \mathrm{Pr}^{1/3}, \tag{8}$$

$$\downarrow$$

$$\mathrm{Sh_{RM}} = 2 + 0.6 \cdot \mathrm{Re}^{1/2} \cdot \mathrm{Sc}^{1/3}. \tag{9}$$

In general, mass transfers around evaporating liquid droplets are best represented with a correction factor due to the mass flow of evaporation (e.g. (Yuen & Chen, 1978)). Also, this correlation calls upon various physical parameters, strongly dependent of the temperature, that need to be correctly evaluated. To do so, in the absence of experimental data, the chosen path is to adjust the macroscopic model with numerical simulations performed with the MESO model, as described below in paragraph 3.2. A critical point is the choice for evaluating the diffusion coefficient, which changes strongly with the temperature along the boundary layer, eq (3).

On the other hand, in the film boiling regime, the formulation can be based on the film thickness as can be calculated from, e.g., (Epstein & Hauser, 1980):

$$\frac{\mathrm{d}\bar{m}_{\mathrm{H_2}}^{\mathrm{FB}}}{\mathrm{d}t} = \frac{D \cdot M_{\mathrm{H_2}}}{\delta} \cdot \frac{p}{R \cdot T_{\mathrm{s}}} \tag{10}$$

Alternatively, in a general way, one could use also a more generic formulation similar to (8), where the film thickness is replaced by $d/\mathrm{Sh_{FB}}$:

$$\frac{\mathrm{d}\bar{m}_{\mathrm{H_2}}^{\mathrm{FB}}}{\mathrm{d}t} = D \cdot M_{\mathrm{H_2}} \cdot \frac{\mathrm{Sh_{FB}}}{d} \cdot \frac{p}{R \cdot T_{\mathrm{s}}} \tag{11}$$

Obviously, oxidation may modify the film boiling characteristics. The use of the Epstein-Hauser correlation will be discussed later on.
Here also the objective is to compare macroscopic model and simulations. However, this task is not fully achieved and we will give here only hints of the progress of this work.

3. MODEL ADJUSTMENT AND VERIFICATION

For the case of droplet in gaseous environment, in the absence of data, it was decided to build and use a numerical simulation model. A comparison is then made between the results given by our subgrid model of oxidation (implemented in MC3D's premixing module PREMIX (Meignen, Picchi, Lamome, Raverdy, Castrillon Escobar, & Nicaise, 2014)) and those extracted from the local scale simulations (run with MC3D's quasi-DNS module MESO).
The MESO model is being improved in order to consider the film boiling configuration. However, only preliminary results will be given here. Furthermore, there exists some experimental data of oxidation rate, although quite imprecise, to adjust the model.

3.1. Description of the DNSs (MESO)

MESO is a quasi-DNS module of MC3D allowing local scale calculations. MC3D is a multiphase flow code based on eulerian modeling with a staggered regular grid (Cartesian or cylindrical), see (Meignen, Picchi, Lamome, Raverdy, Castrillon Escobar, & Nicaise, 2014) for more general information. In the present case, two phases are considered:

- the melt, represented here as a fixed object, that can nevertheless represent conduction and diffusion processes ;
- the gas : a mixture of vapor and hydrogen.

In the present problem, the conduction and diffusion in the melt are not considered (set to very large values). Using a very large heat capacity allows also having a constant melt temperature. The ignoring of the melt temperature changes simply leads to consider a surface temperature driven problem. In reality, there might be a limitation of the heat transfer by conduction and adjustment of surface temperature. This does not modify the physics of the boundary layer as shown by the simulations themselves and the TREPAM experiments (no "history effect"). The adaptation of film boiling to boundary conditions is very fast. Similarly, for the oxidation process, the diffusion coefficient in the melt is set to a very large value so that the dynamics is limited by the diffusion in the gas boundary layer. The reality of this assumption was discussed previously and needs to be strengthened. In the MC3D global model, the actual diffusion (oxidation) is set to the minimum between diffusion in the melt and in the boundary layer, although modeling of diffusion in the melt is still under progress.
The subsequent H_2-H_2O inter-diffusional transport mechanism taking place in the boundary layer is also accompanied by heat transports where both hydrogen and steam carry their own thermal energy to their new location. The mass diffusion flux between cells is written as

$$\phi_{\mathrm{m}} = D_{H_2/H_2O} \cdot M \cdot \frac{\mathrm{d}c}{\mathrm{d}r} \cdot A \ \ (\mathrm{kg/s})$$

where D_{H_2/H_2O} is the diffusion coefficient in eq (3). The associated energy flux is simply given by

$$\phi_{\mathrm{T}} = \phi_{\mathrm{m}} \cdot e.$$

Reference results given by the direct numerical simulations are calculated on a fine 2D cylindrical grid (Fig. 3). The spherical drop is then in fact assimilated to a fixed cylinder situated in the center of a bidimensional transverse flow whose fluid properties are interpolated from steam-water tables as a function of pressure and enthalpy. As the heating object is here a cylinder, a deviation is expected when applied to a sphere. However, for the present purpose, due to the general high uncertainties, the difference is small and neglected.

A particular attention is paid to the surface close region where a refined meshing is necessary to capture the boundary layer. At least 10 meshes are required along the radial direction in the dynamic and thermal boundary layers.

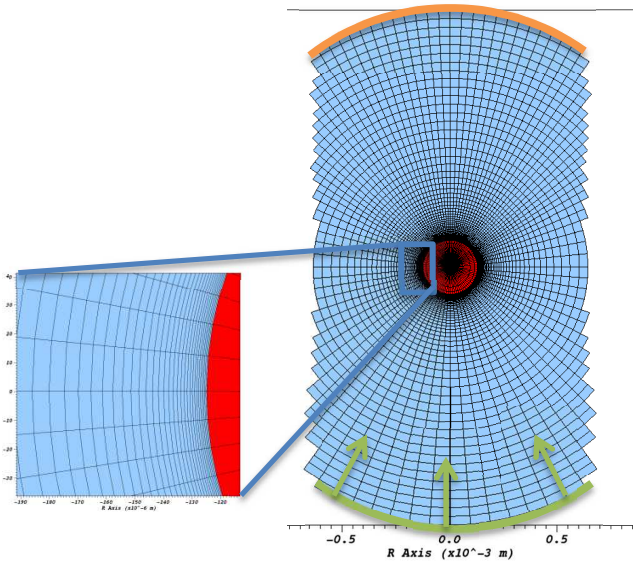

Fig. 3: Example of simulation domain used with MESO. The red represent the cylinder, coarsely meshed here. An inlet condition is applied at the bottom (large green line) and a pressure condition at the top (large orange line). The average inlet velocity is almost one-dimensional.

In compliance with the model's assumptions described earlier, the simulations with MESO provide for the awareness of the rate- limiting H_2-steam inter-diffusion mechanism.

3.2. Vapor Case

A sensitivity study was carried out in which the main parameters are varied over a broad range of values covering those usually encountered in FCIs (table II). All along the calculations, the mass of hydrogen produced is used to deduce the kinetics of oxidation.

The formulation (7) introduced in MC3D-PREMIX model was found, after some few tries, to give acceptable results compared to MESO provided that:
- all properties are evaluated at the average temperature T_m, except:
  - the fluid's density in the Reynolds number that is evaluated at the bulk temperature T_∞, as proposed by (Yuen & Chen, 1978);
  - the diffusion coefficient which is evaluated at the surface temperature T_d ;
- the Sherwood number is adjusted to 50 % of the original formulation as

$$\mathrm{Sh_{vap}} = 1 + 0.3 \cdot \mathrm{Re}^{1/2} \cdot \mathrm{Sc}^{1/3} \qquad (12)$$

Results deduced from the hydrogen productions calculated in the simulations are gathered in table II and plotted in Fig. 4. Calculations were all run up to the same time so that the data can be compared from one case to another one. A value of 100 % · s^{-1} would mean that the drop would be entirely oxidized in 1 s. Deviations reported in table II are on average of 4.6 ± 12.9%, which shows an acceptable agreement of the macroscopic model's results with the DNS.

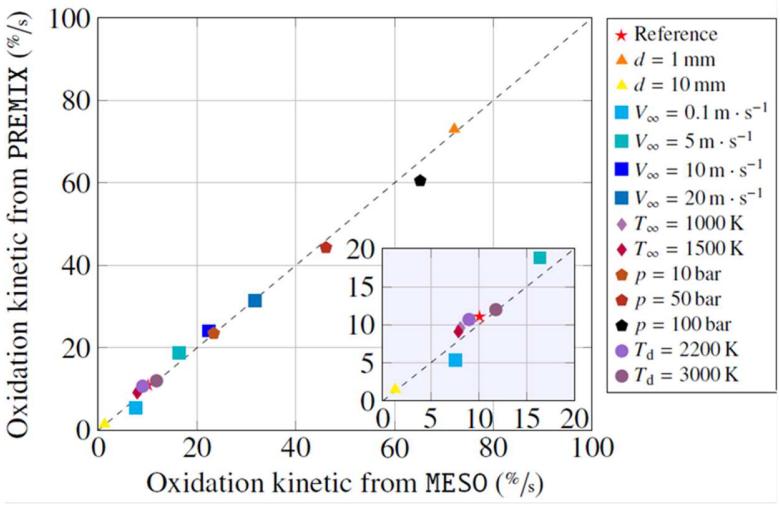

Fig. 4: Comparison between the kinetics of reaction given by the MESO DNS model and the eq (12) introduced in the MC3D-PREMIX application. Inset: magnification of the 0 – 20% zone

The high grades reported in table II clearly indicates the effectiveness of oxidation in the vapor phase during premixing. The comparison among the various points is immediate only for cases with same drop size. The relatively weak impact of the surface (drop) temperature is noticed, in contrast with the impact of the pressure. It is then anticipated that a fine fragmentation under high pressure should lead to a very fast oxidation. In turn, fast oxidation, if accompanied by strong reaction heat (e.g. aluminum or zirconium) should enhance the explosion behavior. A process of "ignition" can then be envisaged. The velocity has also an important effect, which should enhance also this ignition effect.

Table II: Test grid for the vapor configuration and kinetics of oxidation (in percentage of the total oxidation per second) deduced from the PREMIX and MESO calculations. The relative errors based on the results given by the MESO calculations are put in the last column.

Run	**D (mm)**	**V_∞ (m/s)**	**T_∞ (K)**	**p (bar)**	**T_d (K)**	**Varied parameter**	**Ox. Kinetics (% · s^{-1})**		**Error (%)**
							MESO	**PREMIX**	
1	**3**	1	400	1	2500	Reference	10.1	11.2	+10.9
2	**1**	1	400	1	2500	$d = 1$ mm	72.1	73	+1.2
3	**10**	**1**	400	1	2500	$d = 10$ mm	1.3	1.5	+15.4
4	3	**0.1**	400	1	2500	$V_\infty = 0.1$ m/s	7.6	5.4	-29
5	3	**5**	400	1	2500	$V_\infty = 5$ m/s	16.4	18.8	+14.6
6	3	**10**	400	1	2500	$V_\infty = 10$ m/s	22.4	24.1	+7.6
7	3	**20**	**400**	1	2500	$V_\infty = 20$ m/s	31.7	31.5	-0.6
8	3	1	**1000**	1	2500	$T_\infty = 1000$ K	8.1	9.6	+18.5
9	3	1	**1500**	**1**	2500	$T_\infty = 1500$ K	7.9	9.1	+15.2
10	3	1	460	**10**	2500	$p = 10$ bar	23.4	23.5	+0.4
11	3	1	550	**50**	2500	$p = 50$ bar	46.1	44.3	-3.9
12	3	1	600	**100**	**2500**	$p = 100$ bar	65.2	60.5	-7.2
13	3	1	400	1	**2200**	$T_d = 2200$ K	9.0	10.7	+18.9
14	3	1	400	1	**3000**	$T_d = 3000$ K	11.8	12	+1.7

3.3. Film Boiling Case

3.3.1. Preliminary simulations with the macroscopic model of oxidation

The verification process of the macroscopic model in the film boiling configuration is a bit different from that in pure steam as a few experimental data exist in terms of oxidation kinetics. Lemmon Jr et al. (1957) conducted Zr drop experiments in a vertical water tank of controlled temperature. They deduced the rates of reaction from the measurements of the time t_{ox} during which an intense light is emitted by the drop while falling down and the extent of oxidation τ_{ox} of the spherical debris collected after each run. Obviously, a quite high uncertainty is attached to these measurements. Two runs (8 and 9) have been selected from the original experimental series to be numerically reproduced with PREMIX. The experimental conditions and results are given in table III. Very recently, the similar experiments were conducted in the MISTEE installation at KTH (not published yet, see (Ma, Manickam, Guo, & Bechta, 2018), see (Zambaux, Manickam, Meignen, Ma, & Bechta, 2018) for more on MISTEE). The hydrogen production was based on the estimate of the bubble production, supposed to be rapidly at equilibrium, so with also a noticeable uncertainty. In conditions similar to the run 8 in table III, an oxidation rate of about 35 % was estimated, with however a faster kinetics of about 10%/s.

Table II: Experimental conditions and results from Lemmon Jr. et al. [5] that have been used in the simulations. Extents of oxidation reported are those obtained by weight increase measurement. The drop diameter d is deduced from the mass m_d of the debris, supposing that they are spherical.

Run	T_∞ **(K)**	p **(bar)**	T_d **(K)**	t_{ox} **(s)**	ΔV_∞ **(m/s)**	m_d **(g)**	d **(mm)**	τ_{ox} **(%)**
8	338.0	1	2173	6.20	0.73	0.59	5.6	36.8
9	366.5	1	2173	9.25	0.71	0.62	5.7	44.1

The calculated time evolutions of oxidation along with the drop temperature have been plotted in Fig. 5for the two runs. The first observation that can be drawn from this figure is that predicted kinetics of reaction is of the order of magnitude but faster than that measured experimentally. However, the calculation is quite consistent with the most recent data. Mean drop temperatures are observed to increase until equilibrium is found with the heat losses resulting in a plateau. During this process, no significant variations in the kinetics of oxidation are noticed. It will be noticed that the drops in the MISTEE tests, reached the bottom of the tank rapidly, while remaining in a somewhat round shape, so, likely, almost solid. This indicates that the drop may have not reached the high temperature calculated in run 8, thus confirming the probably too fast oxidation rate.

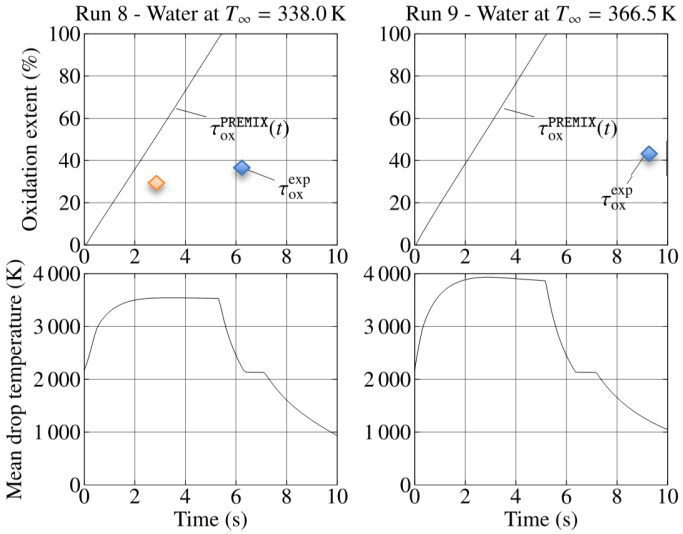

Fig. 5: Temporal evolutions of the kinetics of oxidation and mean drop temperatures calculated with the macroscopic model and compared to the data by (Lemmon Jr., Crooks, Hershall, Sorgenti, & Filbert Jr., 1957), blue diamonds, and (Ma, Manickam, Guo, & Bechta, 2018), orange diamond.

3.3.2. DNSs of the film boiling configuration

In an attempt to adjust more precisely the kinetics of oxidation in the film boiling configuration, the following stage thus consists in performing DNSs with MESO, similarly to what was done for the gas configuration. Here, we will only give a brief status of the work as it is still in a preliminary phase. As stated previously, in the current MESO model, only one field is used to calculate both the liquid water (when the temperature is below saturation) and steam (when the temperature is above saturation). Around the saturation temperature, a mixture of liquid and vapor is considered at local equilibrium. Due to this single-fluid formulation, MESO simulations of film boiling are more easily carried out in high pressure conditions, where the differences in the fluid's physical properties between the liquid and vapor states are much less significant than those at low pressure. A 2-phase formulation is foreseen to be able to evaluate situations at low pressure. Nonetheless, liquid/liquid configuration is most important in explosion configuration, i.e. at high pressures. In a side work (Meignen, Piluso, & Rimbert, 2017)simulations of film boiling in the pressure range [5-100] MPa were done, indicating that film boiling under such conditions could be approximately reproduced by standard film boiling correlations as those integrated in the MC3D code, as well as results from TREPAM experiments (Berthoud & Gros D'Aillon, 2009) . An example of calculations is given in Fig. 6. The MESO calculation compares well with the test experimental data and is in the range of the tested correlations. It may however be noticed from this figure that the Epstein-Hauser correlation used as first guess for the model over-predicts in general the heat transfer.

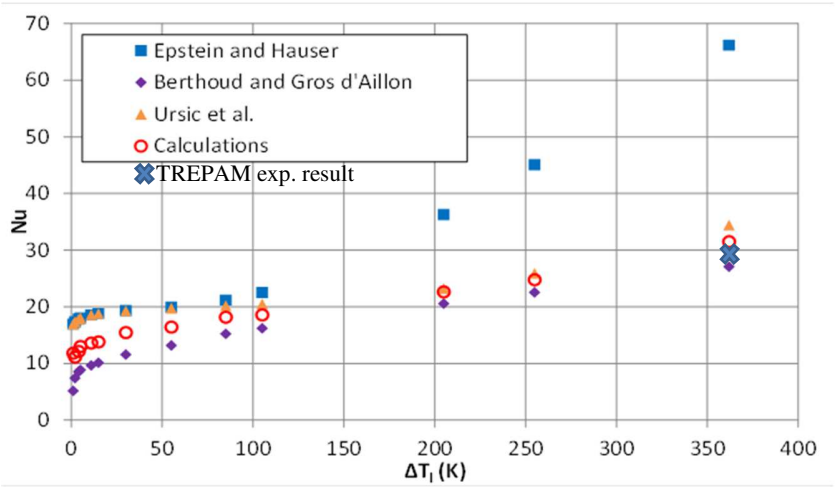

Fig. 6: Comparison of the heat transfer calculated from the numerical simulations and the heat transfer given by three film boiling correlations and a result from the TREPAM test, at 24 MPa and high subcooling.

It is also clear that the oxidation should modify the transfer and film characteristics.
Only simulations in supercritical pressure conditions are here considered. In this domain, pseudo film boiling may be observed and the fluid does exhibit a high density pseudo-liquid state and low density pseudo-vapor state. An example of first performed simulations is given here below for a case at 100 MPa run with oxidation either enabled (case A1) or disabled (A2). The drop temperature (2150 K) is maintained fixed all along the simulations which are run for a typical explosion time of 3 ms. It is worth noting that in these simulations the reaction does not generate any heat and the cooling is neither taken into account (the drop has a fixed temperature). The inlet fluid temperature is 750 K, i.e. with a rather small but substantial water subcooling (54 K). The fluid density fields are compared Fig. 7. The contours of hydrogen fraction are shown in Fig. 8. We find that, at the examined time scale here, a quasi-steady situation is rapidly reached. The equivalent volume of (gas) is not so different from A1 to A2. The film thicknesses measured at the stagnation point (δ_{SP}) and at the equator (δ_{EQ}) are gathered in table IV, compared with that given by the Epstein-Hauser correlation. In the absence of oxidation, the Epstein-Hauser correlation leads to a somewhat reduced film thickness, as already commented before. But, although this correlation is not dedicated to films comporting hydrogen, the order of magnitude of the calculated values remains quite satisfactory. It is also verified that the hydrogen boundary layer is embedded in the thermal one. Thus, along the pseudo-interface, the hydrogen fraction is effectively very small, as hypothesized in the model, eq. (10).

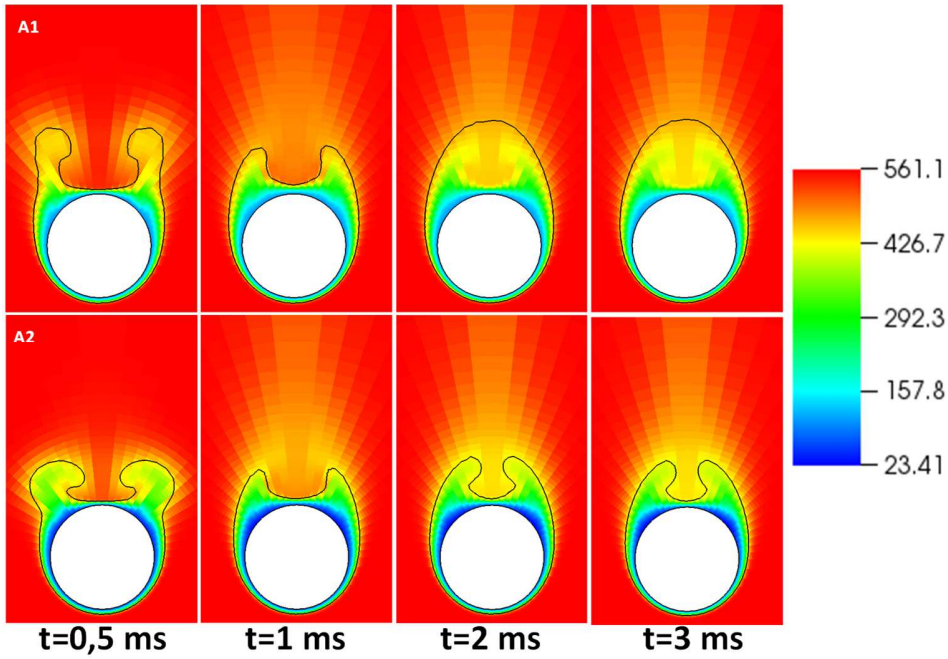

Fig. 7: Snapshots of the fluid density field around the drop for the two cases without oxidation (A1, top) and with (A2, bottom). Red is for the fluid high density zones (liquid water); Blue is for the low density regions (gas). The black line marks the contour of saturation temperature.

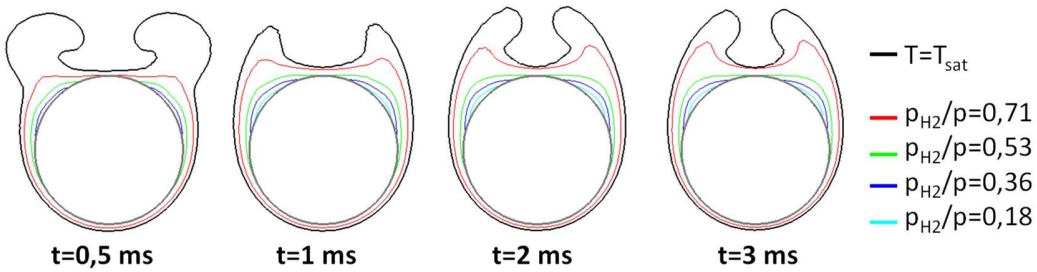

Fig. 8: Visualization of the 2D contours of hydrogen fraction and contour of saturation temperature (at total pressure) (simulation A2).

Finally, one can compare the oxidation kinetics from the hypothesized formulation (10) with that obtained using MESO DNS, Fig. 9. Following the conclusions of previous section, the diffusivity might be computed at the surface temperature. This approximately doubles the oxidation rate compared to the standard assumption of using a mean temperature. It is seen that the MESO oxidation rate is in the same range, although notably smaller. These results are to be compared also with those reported in Fig. 5(at ambient pressure and spherical geometry). Although additional work is needed, in the three directions of DNS simulation, macro modeling and experiments, these results are encouraging and should lead to the derivation of an adjusted oxidation rate in near future. At the moment, the use of the formulation (10), with diffusion coefficient evaluated at a mean film temperature may be used for preliminary evaluations.

Table IV: Measurement of the film at different locations around the drop. δ_{SP}: film thickness at the upstream stagnation point; δ_{EH}: film thickness evaluated with the Epstein-Hauser correlation; δ_{EQ}: film thickness at the drop equator.

Run	δ_{SP} (mm)	δ_{EH} (mm)	δ_{EQ} (mm)
A1	0.012	0.014	0.025
A2	0.011	0.016[a]	0.020

[a]: Considering a film composition of 50% steam and 50% hydrogen.

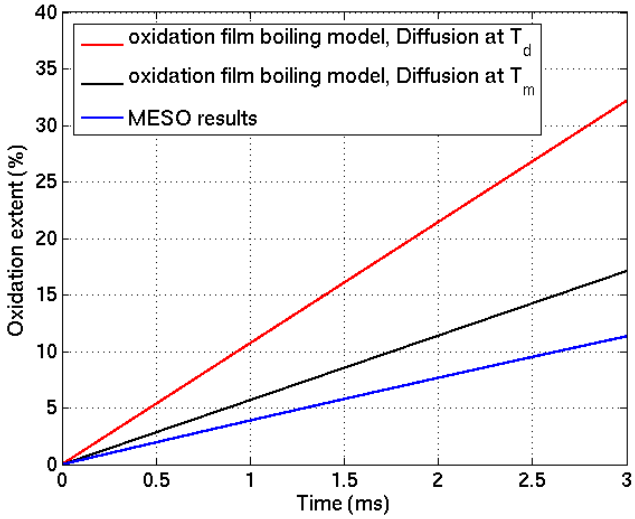

Fig. 9: Comparison of the hydrogen production from the preliminary proposal (10), considering two temperatures for the evaluation of diffusivity, with the MESO model result for the case A2.

4. CONCLUSIONS

In this work, a macroscopic model of oxidation based on the assumption that the H_2-steam inter-diffusion is the rate-limiting mechanism is being derived for the FCI code MC3D for both premixing and explosion conditions. This model intends to describe the oxidation rate as long as the drop is liquid. In such case, it is likely that diffusion is very fast in the melt and thus the limiting process of oxidation is the diffusion in the gaseous boundary layer. In case of quenching and appearance of solidification, diffusion limitation in the melt may be considered thanks to available data. Two drop configurations are considered: the liquid/gas configuration, likely to be more representative for oxidation during premixing, and the liquid/liquid film boiling configuration, likely to be more representative for explosion. In order to verify/adjust the models, a quasi-DNS model has been built and is used to supplement the current lack of precise experimental data. The work is still in a preliminary status and first outcomes are given.

For the liquid/gas system, for which no data could be found, the DNS's allow a qualitative verification and quantitative adjustment of the proposed correlation, eq (12). The model already allows identifying a possible ignition/escalation effect during an explosion due to the strong impact of pressure and ambient velocity.

For the case of liquid/liquid configuration, one has preliminarily used some experimental data of zirconium oxidation. To complement the analysis, the work has been oriented towards the use of the DNS technic. Only preliminary results are shown here. They are nevertheless encouraging for the derivation of an adequate correlation. The next step is then related to the continuation of the DNS work to build a reliable correlation, before confronting to the available experimental data related to steam explosion.

Quite important efforts are however still needed to achieve the development of a full validated model of oxidation and its impact on FCI. In particular, over the course of this study, taking into account the variations of the material physical properties due to oxidation has become an important perspective. The melt energy as well as the entire oxidation process intimately depends on this feature. Solidification will be strongly affected. Thus, the final step will be to deduce the solidification mechanism from DNSs. We nevertheless encourage experimental work for both liquid/gas and liquid/liquid conditions. At that point, we can cite current efforts underway by both CEA and KTH institutes.

NOMENCLATURE

δ : film thickness (m)
ΔH_{r} : enthalpy of reaction (J/mol)
ρ : density (kg/m^3)
τ_{ox} : extent of oxidation (%)
$c_{\mathrm{H_2}}$: hydrogen molar concentration (mol/m^3)
c_{p} : heat capacity (J/kg/K)
d : drop diameter (m)
D : H_2-steam diffusion coefficient (m^2/s)
L_c : characteristic length used in the correlation (m)
M : molar mass (kg/mol)
p : total pressure (Pa)
$p_{\mathrm{H_2}}$: hydrogen partial pressure (Pa)
r : radial coordinate from the drop surface
t : time or duration (s)
T : temperature (K)
V : velocity (m/s)
ΔV : velocity difference (m/s)

Other symbols and subscripts are self-explanatory.

ACKNOWLEDGMENTS

This work is done in the frame of French RSNR-ICE research program on FCI. The authors acknowledge the sponsors of the ICE program, namely EDF, AREVA and the French Government through the Research National Agency (ANR). We also thank other participants in the RSNR-ICE program, from CEA and the University of Lorraine for their valuable comments on this work.
Many thanks also to Severe Accident KTH team, particularly Sevostian Bechta and Weimin Ma, for valuable discussions and works on the MISTEE-Zr tests. We also acknowledge Marc Barrachin and Bruno Piar, IRSN, for their support.

REFERENCES

Baker Jr, C., & Just, C. (1962). Studies of metal-water reactions at high temperatures. III. Experimental and theoretical studies of the Zirconium-water reaction. *Technical Report ANL-6548, Argonne National Laboratory*.

Barrachin, M., Chevalier, P., Cheynet, B., & Fischer, E. (2008). New modelling of the U–O–Zr phase diagram in the hyper-stoichiometric region and consequences for the fuel rod liquefaction in oxidising conditions. *Journal of Nuclear Materials 375*, 397–409.

Berthinier, C., Rado, C., Chatillon, C., & Hodaj, F. (2013). Thermodynamic assessment of oxygen diffusion in non-stoichiometric UO2±x. *Journal of Nuclear Materials 433*, 265–286.

Berthoud, G., & Gros D'Aillon, L. (2009). Film boiling heat transfer around a very high temperature thin wire immersed into water at pressure from 1 to 210 bar: Experimental results and analysis. *International Journal of Thermal Sciences, vol 48*, 1728-1740.

Bostrom, A. W. (1954). The high temperature oxidation of zirconium in water. *Technical Report WAPD-104, Westinghouse Atomic Power Division*.

Breitung, W. (1978). Oxygen self and chemical diffusion coefficients in UO2±x. *Journal of Nuclear Materials 75*, 10-18.

Cho, D., Armstrong, D., & Gunther, W. (1998). Experiments on interactions between zirconium-containing melt and water. *NUREG/CR-5372*.

Corradini, M. L., Mitchell, D., & Evans, N. A. (1983). Hydrogen generation during a core melt-coolant interaction. *Proc. Int. Mtg. Light Water Reactor Severe Accident Evaluation, 1*.

Epstein, M., & Hauser, G. M. (1980). Subcooled forced-convection film boiling in the forward stagnation region of a sphere or cylinder. *International Journal of Heat and Mass Transfer, vol. 23*, 179–189.

Epstein, M., Fauske, H., & Theofanous, T. G. (2000). On the mechanism of aluminum ignition in steam explosions. *Nuclear Engineering and Design, vol. 201*, 71–82.

Epstein, M., Leung, J. C., Hauser, G. M., & Henry, R. E. (1984). Film boiling on a reactive surface. *International Journal of Heat and Mass Transfer, vol 27(8)*, 1365–1378.

Fichot, F., Carénini, L., Sangiorgi, M., Hermsmeyer, S., Miassoedov, A., Bechta, S., et al. (2018). Some considerations to improve the methodology to assess In-Vessel Retention strategy for high-power reactors. *Annals of Nuclear Energy 119*, 36-45.

Furman, S. C., & Epstein, L. F. (1959). *Metal-water reactions : V. the kinetics of metal-water reactions, low pressure studies.* GEAP-3208, Vallecitos Atomic Laboratory. General Electric Company.

Lee, B. C., Park, G. C., & Chung, C. H. (1997). Development of a mechanistic model for hydrogen generation in fuel-coolant interactions. *Journal of the Korean Nuclear Society, vol. 29(2)*, 99-109.

Lemmon Jr., A. W., Crooks, R. C., Hershall, P. G., Sorgenti, H. A., & Filbert Jr., R. B. (1957). Studies relating to the reaction between zirconium and water at high temperatures. *Technical Report BMI-1154, Battelle Memorial Institute*.

Ma, W., Manickam, L., Guo, Q., & Bechta, S. (2018, April 18-20). *MISTEE Investigation on Mechanisms of Steam Explosion during Severe Accidents.* 5th NUGENIA-SARNET TA2.2 Review Meeting, Puerto de La Cruz, Spain.

Magallon, D., Huhtiniemi, I., & Hohmann, H. (1999). Lessons learnt from FARO/TERMOS corium melt quenching experiments. *Nuclear Engineering and Design, 189*, 223-238.

Mastromarino, S., Seibert, A., Hashem, E., Ciccioli, A., Prieur, D., Scheinost, A., et al. (2017). Assessment of solid/liquid equilibria in the (U, Zr)O2+y system. *Journal of Nuclear Materials 494*, 368-379.

Meignen, R., & et al. (2014). Status of steam explosion understanding and modelling. *Annals of Nuclear Energy, Volume 74*, 125-133.

Meignen, R., Picchi, S., Lamome, J., Raverdy, B., Castrillon Escobar, S., & Nicaise, G. (2014). The challenge of modeling fuel-coolant interaction: Part I - Premixing. *Nuclear Engineering and Design, 280*, 511–527.

Meignen, R., Piluso, P., & Rimbert, N. (2017, Sept 3-8). Outcomes of the French ICE project on Fuel Coolant Interaction. *The 17th International Topical Meeting on Nuclear Reactor Thermal Hydraulics (NURETH-17).* Qujiang Int'l Conference Center, Xi'an, China.

Meignen, R., Raverdy, B., Picchi, S., & Lamome, J. (2014). The challenge of modeling Fuel Coolant Interaction: part II– explosion. *Nuclear Engineering and Design, Volume 280*, 528-541.

Nelson, L. S. (1995). Steam explosions of single drops of pure and alloyed molten aluminum. *Nuclear Engineering and Design, vol. 155, Issues 1–2*, 413-425.

Ranz, W. E., & Marschall, W. R. (1952). Evaporation from drops. *Chem. Eng. Prog., vol. 48(22)*, 141–146.

Spencer, B. W., Wang, K., Blomquist, L. M., McUmber, L. M., & Schneider, J. I. (1994). Fragmentation and quench behavior of corium melt streams in water. *NUREG/CR-6133, ANL-93-62*.

Turney, D., & Banerjee, S. (2013). Air–water gas transfer and near-surface motions. *J. Fluid Mech. 733*, 588–624.

Tyrpekl, V., Piluso, P., Bakardjieva, S., Niznansky, D., Rehspringer, J.-L., Bezdicka, P., et al. (2015). Prototypic corium oxidation and hydrogen release. *Annals of Nuclear Energy*, 210–218.

Uršič, M., Leskovar, M., & Meignen, R. (2015). Eulerian modelling of melt solidification impact during fuel–coolant interaction. *Annals of Nuclear Energy, volume 78*, 130-139.

Yakub, E., Ronchi, C., & Staicu, D. (2007). Molecular dynamics simulation of premelting and melting phase transition in stoichiometric uranium dioxide. *Journal of chemical Physics, 127(9).*

Young, M. F., Berman, M., & Pong, T. L. (1988). Hydrogen generation during fuel/coolant interactions. *Nuclear Science and Engineering, vol. 98*, 1-15.

Yuen, M. C., & Chen, L. W. (1978). Heat-Transfer measurements of evaporating liquid droplets. *Int. J. Heat and Mass transfer, Vol.21*, 537-542.

Zambaux, J., Manickam, L., Meignen, R., Ma, W., & Bechta, S. (2018). Study on thermal fragmentation characteristics of a superheated alumina droplet. *Annals of Nuclear Energy, 119*, 352-361.